and B) were included at 808nm. The weak spectral features on the high wavelength side of some reflection peaks have been confirmed using a narrow-line tunable Ti-sapphire laser and may indicate the presence of a weak but distinct transverse mode in the excimer laser beam. The spectrum of the array after embedding is shown in Fig. 2*b*. For clarity, external strain was applied to grating B to move it away from grating A, which is used as the reference grating. The λ_Bs of the seven embedded gratings (C–I) have all increased due to inadvertent tensile stress (> 1% for gratings G and H) from unequal feed rates on the optical fibre and the fabric as they entered the die; this differential stress was locked in by the resin cure. The shift in λ_B of grating C is much less than that of gratings D–I, and the shifts among the latter group are not equal, indicating nonuniform stress along the length of the panel. In addition, there is evidence of nonuniform stress across the gauge length of some sensors, e.g. gratings F–I, which causes their reflection peaks to distort and decrease in amplitude, likely due to roughness in the texture of the fibreglass plies on a scale smaller than the FBG length.

The composite panel was supported on rollers located approximately under gratings C and I and placed in three-point bending using various weights. The spectrum of the embedded FBG array was measured, and each of the sensors between the pivots showed a decrease in λ_B due to the compressive strain induced in the gratings, located on the concave side of the panel.

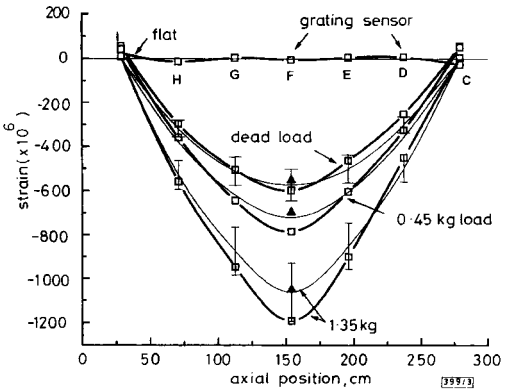

Fig. 3 *Comparison of strain in CRTM™ beam measured with FBG sensors and results of finite element and analytical calculations*

Uncertainty bars on the FEA data are due to uncertainty in the position of the sensors relative to the neutral axis

—□— experimental
——— FEA
▲ analytical, calculation

Axial strains were estimated from the λ_B shifts of each of the FBGs (assuming $1/\lambda_B d\lambda/d\varepsilon = 0.74$ and uniaxial stress), and these data are plotted in Fig. 3. To accurately determine the wavelength shift of each grating, its individual reflectance spectrum in the 'flat' supported case (Fig. 2*b*) was first fit by the sum of 2–4 Gaussians. This calculated spectrum was then translated in wavelength for best correlation with the measured spectrum of that grating in each of the strained cases. This correlation method gives a resultant error of < 1/4 pixel = 0.1Å = 17με. Note that the measurement accuracy is degraded for gratings HI and I, which have weak reflectance spectra that are overlapped in some of the loaded cases.

The experimental results are compared in Fig. 3 with the results of two calculations: the beam midpoint strains being calculated analytically from the measured deflected shape of the beam and nonlinear finite element analysis (FEA) performed using COSMOS/M. There is excellent agreement between the two calculations, while there is some variance between the experiment and calculated strains, which can be reasonably attributed to variations of ±1/2 ply thickness (0.276mm) in the position of the sensor relative to the neutral axis. The fabric used in this experiment is quite thick and irregular, and it is not uncommon for *in-situ* sensors to be displaced into the weave of the fabric during CRTM™ processing. This depth uncertainty can result in as much as a 12.5% uncertainty in calculated strain, as shown by the bars on the FEA results in Fig. 3, but all measured strains fall within the uncertainty. For typical deep section structural members, such as 'I' and 'C' beams with embedded FBG sensors in the flanges, the strain uncertainty from ±1/2 ply thickness mislocation would be much less due to the larger distance from the neutral axis in comparison to the ply thickness, e.g. < 0.5% at one ply depth below the surface for a 30 cm deep flange. Another source of error may be the conversion of wavelength shift to strain, which assumes a uniaxial stress state that is generally not the case in embedded optical fibres [4].

Summary: This Letter reports initial results of embedding FBG sensor arrays produced on-line during optical fibre drawing in a fibre-resin composite using the CRTM™ process. The strain distribution of the beam under three-point bending has been determined from shifts in λ_B, and the measured strains compare favourably with calculated results. This study establishes the potential of fabricating low-cost fibre-reinforced composite smart structural elements with embedded optical fibre sensors.

Acknowledgments: The authors wish to thank J.S. Sirkis for helpful discussions and acknowledge the financial support of ARPA under the Affordable Polymeric Composite Material Synthesis and Processing program in accordance with ARPA Technology Agreement No. MDA972-93-2-0004.

24 August 1994

Electronics Letters Online No: 19941180

E. J. Friebele, C. G. Askins and M. A. Putnam (*Naval Research Laboratory, Washington, DC 20375, USA*)

A. A. Fosha, Jr., J. Florio, Jr., R.P. Donti and R. G. Blosser (*BP Chemicals, Inc. Auburn, WA 98002, USA*)

References

1 ASKINS, C.G., PUTNAM, M.A., WILLIAMS, G.M., and FRIEBELE, E.J.: 'Stepped-wavelength optical-fiber Bragg grating arrays fabricated in line on a draw tower', *Opt. Lett.*, 1994, **19**, pp. 147–149

2 ASKINS, C.G., PUTNAM, M.A., WILLIAMS,S G.M., and FRIEBELE, E.J.: 'Continuous fiber Bragg grating arrays produced on-line during fiber draw', *in* SIRKIS, J.S. (Ed): 'Smart sensing, processing, and instrumentation. Vol. 2191' (SPIE, Bellingham, QA, 1994), pp. 80–85

3 KERSEY, A.D., BERKOFF, T.A., and MOREY, W.W.: 'Multiplexed fiber Bragg grating sensor system with a fiber Fabry Perot wavelength filter', *Opt. Lett.*, 1993, **18**, pp. 1370–1372

4 SIRKIS, J.S.: 'Unified approach to phase-strain-temperature models for smart structure interferometric optical fiber sensors: Part 1, development', *Opt. Eng.*, 1993, **32**, pp. 752–761

Low skew multimode ribbon fibres for parallel optical communication

S. Siala, A.P. Kanjamala, R.N. Nottenburg and A.F.J. Levi

Indexing term: Optical cables

Interchannel skew in graded index multimode fibre-optic ribbon can be reduced by forming each channel from fibre sequentially cut from the same pull. A 1.25ps/m maximum variation in optical pulse delay has been measured across a 102m long 12fibre ribbon. These improvements extend the applications of multimode ribbon fibre to include low cost synchronous parallel transmission at 622Mbyte/s over distances greater than 1 km.

Robust, low-cost gigabit per second fibre-optic links operating at 1.3 or 0.78μm wavelengths are needed to satisfy existing and future system requirements. Parallel links based on fibre ribbon have been suggested for high density/throughput interconnects in advanced switching and computing systems [1]. Assuming production volumes of 100000 12-wide transmitter and receiver units per

year it is possible to evaluate link price. In such quantity, jacketed fibre is $0.25/m/fibre. Precision transfer moulded plastic 12-wide MT fibre array push-on connectors from US Conec are $25 each assembled and attached. Hence, a 12-wide connectorised 10 m long jumper cable is $80. Gigabit per second transmitter and receiver modules connectorised to multimode MM fibre are approximately $200 each assembled and tested. Thus, a 12-wide multigigabit per second fibre-optic link with a 10m jumper cable is less than $500. These modest prices are possible because low cost fibre and connector technologies exist and also because of relaxed alignment tolerance due to use of 62.5 or 50μm diameter core MM fibre in the module.

However, an important factor limiting the range of potential applications for parallel optic links based on MM fibre is variation in signal propagation delay between fibre channels. Such interchannel skew is due to variation in the refractive index of fibres forming the ribbon. The purpose of this Letter is to quantify this experimentally and thereby set a practical maximum limit to bandwidth-distance product per channel of low-cost parallel MM fibre links.

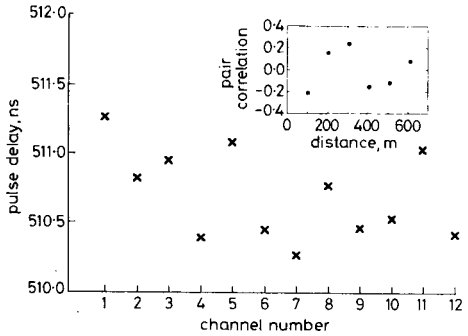

Fig. 1 *Measured optical pulse delay after transmission through 103m of conventional 12channel optical ribbon fibre, resulting in maximum interchannel skew of 1005ps*

Average delay is 510.696ns, maximum delay is 511.259ns, minimum delay is 510.254ns, and standard deviation is 0.328ns or 3.18ps/m

The ribbon fibre described here consists of an array of 12 MM graded-index glass fibres spaced 250μm apart with core diameter 62.5μm. The MT terminated ribbon fibre has a total length of ~100m and each connector has an insertion loss of 0.327 +/- 0.05dB [2]. Using the same Fabry Perot laser with emission at λ = 1.3μm wavelength, a fast detector, and a high-speed oscilloscope, interchannel skew across the ribbon fibre is accurately determined. The cumulative error in this measurement, which is mostly due to timing jitter, is about 1 part in 10^5. In Fig. 1 we show results of measuring propagation delay in a conventional ribbon fibre. As may be seen, skew between channels is characterised by a standard deviation σ = 3.2ps/m, and a maximum skew of approximately 10ps/m or 1005ps over the 103m length of the 12 fibre ribbon. A measure of interchannel skew correlation is given by the pair correlation function

$$r_d = \frac{\frac{1}{n}\sum_i\{(x_i - \eta_x)(y_i - \eta_y)\}}{\sigma_x \sigma_y}$$

where r_d is the correlation coefficient, n the number of correlation points, x_i the delay for the first set of channels, y_i the delay for the second set of channels which are the dth nearest neighbour of x_i, respectively, and η_x (η_y) and σ_x (σ_y) are the mean and standard deviation of x_i (y_i), respectively. The insert in Fig. 1 shows that skew is uncorrelated for conventional ribbon fibre.

Fig. 2 shows the results of measuring the propagation delay in high quality graded index MM fibre manufactured by Corning and sequentially cut from the same pull. This process results in correlations between the effective refractive index for each fibre in the ribbon. The measured maximum variation in optical pulse delay across the 12 fibre ribbon is 1.25ps/m/12-fibres or 127ps over the 102m length of the ribbon with a standard deviation σ = 0.39ps/m. To our knowledge, this skew is the lowest reported for a 12-fibre ribbon. As expected, the insert to Fig. 2 shows that a correlation in skew exists and decreases with increasing distance separating the fibre sections being compared. Reduced variation in fibre composition during the manufacturing process will increase this correlation and result in a further reduction in skew.

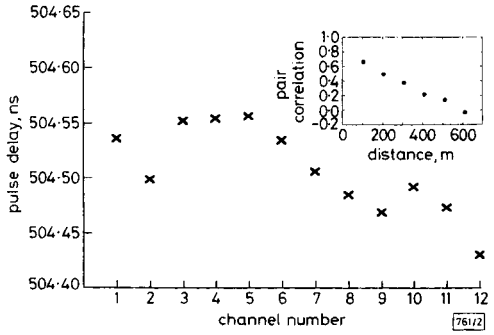

Fig. 2 *Pulse delay after transmission through 102m of 12channel ribbon fibre manufactured from high quality graded index MM fibre sequentially cut from the same pull*

The measured maximum interchannel skew is 127ps. Average delay is 504.508ns, maximum delay is 504.557ns, minimum delay is 504.430ns, and standard deviation is 0.040ns or 0.392ps/m

Compared to singlemode (SM) fibre, MM fibre has the advantage of relaxed optical alignment tolerances (by a factor of ~10) in a transceiver module assembly and much better coupling efficiency (which reduces the electrical gain requirements of the receiver). For synchronous parallel optical links, SM fibre loses its intrinsically higher bandwidth-distance advantage when interchannel skew of the ribbon becomes the limiting factor. For instance, a skew of 2.1ps/m in 8fibre SM ribbon, as reported in [3], would limit the synchronous connection distance to less than 500m at 1Gbit/s. Our low skew MM ribbon fibre avoids the use of costly optical or electronic skew-correcting components [4] and is at least as good as SM fibre in satisfying the bandwidth-distance/channel requirements of low cost synchronous parallel links.

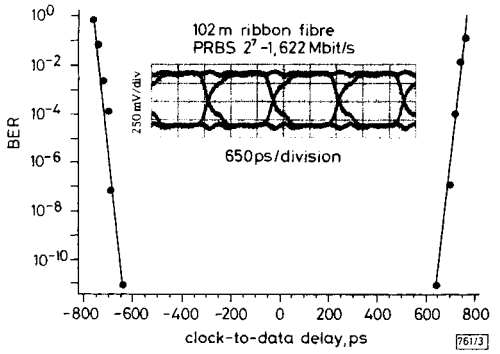

Fig. 3 *Eye diagram and BER against clock-to-data delay of parallel synchronous digital transmission over 102m of low skew MM ribbon fibre at 622Mbit/s with 27^{-1} NRZ PRBS*

Inset: eye diagram

We measured bit error rate (BER) against clock-to-data delay for synchronous parallel transmission at a data rate of 622Mbit/s. Two channels (one for clock, one for data) of a laser array transmitter module operating at λ = 0.98μm wavelength were used [5], along with a 12channel DC-coupled digital optical receiver module [6]. The inset of Fig. 3 shows the eye diagram obtained with the low skew 102 m long MM ribbon fibre for a 622Mbit/s non-return-to zero (NRZ) 2^7–1 pseudorandom bit stream (PRBS). As shown in Fig. 3, a clock-to-data delay of up to 1.3ns can be tolerated while keeping the BER less than 10^{-11}. Thus, the 12channel transmission span over this very low skew ribbon fibre at 622Mbit/s/channel with $BER < 10^{-11}$ can be increased to a maximum of ~1km. The maximum 8channel transmission span with an aggregate data rate of 622Mbyte/s should be greater than 1km.

This increase in transmission distance is very important in data communication applications such as computer-to-computer interconnections in local area networks and also for future high-speed local loops linking switching terminals to curbside distribution boxes (fibre-coax distribution) for broadband digital services to the home.

© IEE 1994
5 July 1994
Electronics Letters Online No: 19941190

S. Siala, A. P. Kanjamala, R. N. Nottenburg and A. F. J. Levi (*Department of Electrical Engineering-Electrophysics, University of Southern California Los Angeles, California 90089-1112, USA*)

References

1 NORDIN, R.A., LEVI, A.F.J., NOTTENBURG, R.N., O'GORMAN, J., TANBUN-EK, T., and LOGAN, R.A.: 'A systems perspective on digital interconnection technology', *J. Lightwave Technol.*, 1992, **LT-10**, pp. 811–827

2 SATAKE, T., ARIKAWA, T., BLUBAUGH, W.P., PARSON, C., and UCHIDA, T.K.: 'MT multifiber connectors and new applications', Proc. 44th Electronic Components & Technology Conf., 1994, (Washington DC), pp. 994–999 (IEEE cat#94CH3241-7, ISBN#0-7803-0914-6)

3 TAKAI, A., KATO, T., YAMASHITA, S., HANATANI, S., MOTEGI, Y., ITO, K., ABE, H., and KODERA, H.: '200-Mb/s/ch 100-m optical subsystem interconnections using 8-channel 1.3μm laser diode arrays and single-mode fiber arrays', *J. Lightwave Technol.*, 1994, **LT-12**, pp. 260–269

4 HORIMATSU, T., FUJIMOTO, N., WAKAO, K., and YANO, M.: 'Optical parallel interconnection based on group multiplexing and coding technique', *IEICE Trans. Electron.*, 1994, **E77-C**, pp. 35–41

5 SIALA, S., ZHAO, H., GOVINDARAJAN, M., NOTTENBURG, R.N., and DAPKUS, P.D.: 'High-speed large signal digital modulation of three-terminal low-threshold strained InGaAs/GaAs lasers', to be published in *IEEE Photonics Technol. Lett.*, 1994, **6**, (6)

6 GOVINDARAJAN, M., SIALA, S., and NOTTENBURG, R.N.: '12 × 622Mb/s DC-coupled synchronous optical receiver array for parallel digital datalinks', *Electron. Lett.*, 1994, **30**, (14), pp. 1177–1178

Simultaneous strain and temperature sensing employing a photogenerated polarisation coupler and low-order modes in an elliptically cored optical fibre

S.E. Kanellopoulos, V.A. Handerek and A. J. Rojers

Indexing terms: Fibre optic sensors, Photorefractive effect, Optical fibre polarisation, Optical couplers, Strain measurement, Temperature measurement

A new technique is demonstrated for simultaneous strain and temperature sensing using a fibre polarisation coupler in an elliptically cored optical fibre carrying only a few low-order modes. The applied strain and temperature can be determined from the effect that they have on the resonant coupling wavelengths for the orthogonal polarisation states of the fundamental and first higher order modes.

Introduction: Simultaneous sensing of strain and temperature has recently been achieved in several ways. One approach uses combined polarimetric-interferometric techniques, employing the polarisation properties of the fundamental mode and the first higher order modes of a fibre [1, 2]. Elliptically cored fibres have long been used in some of these bimodal sensing schemes because the ellipticity breaks the modal degeneracy associated with a circular core, resulting in azimuthally stable field distributions for the higher order modes [3–7].

In this Letter, we present a different method by which strain and temperature can be determined simultaneously. The technique makes use of a polarisation coupler (or rocking filter) in an overmoded, elliptically cored fibre. The first four higher order modes for a core ellipticity close to 0.5 are the ${}_eHE_{01}$, ${}_oEH_{01}$, ${}_eHE_{21}$ and ${}_oHE_{21}$ modes. In the weakly guiding approximation for circularly cored fibre these modes are nearly degenerate, having almost identical propagation constants. In elliptically cored fibre this degeneracy is lifted, leading to two pairs of modes grouped by mode order and with the electric field of either member of any pair being orthogonally polarised with respect to its twin. The polarisation coupler converts power only within any pair, including the fundamental (${}_eHE_{11} \leftrightarrow {}_oHE_{11}$) and higher order groups (${}_eHE_{01} \leftrightarrow {}_oEH_{01}$, ${}_eHE_{21} \leftrightarrow {}_oHE_{21}$). Each pair of modes exhibits a different resonant coupling wavelength [8, 9] due to its unique spectral variation of beatlength compared to the remaining pairs. Conversely, each pair of modes will exhibit a given polarisation beatlength at differing wavelengths. In some circumstances, these wavelengths can be very similar for some pairs of modes. The proposed method relies on the differing dependences on strain and temperature of the modal birefringence for these lowest-order modes. These measurands can be determined simultaneously from the effects which they have on the resonant coupling wavelengths associated with two pairs of modes. We have previously demonstrated simultaneous strain and temperature sensing using overlaid gratings of different types acting on the fundamental mode alone [12]. In comparison with that approach, the method described here clearly offers a simpler sensor fabrication procedure. This method also avoids the potential complications involved with the use of Bragg gratings, which have also recently been used to perform simultaneous strain and temperature sensing [13].

Theory: The resonant condition for a polarisation rocking filter is given by $\lambda_i = \delta n_i \Lambda$, where λ_i is the resonant coupling wavelength for each pair of modes ($i = 1$ corresponds to the fundamental and $i = 2$ to the first higher order pair), δn_i is the modal birefringence of the ith pair and Λ is the grating period, equal to the relevant polarisation beatlength. The fractional change in the resonance wavelength for each pair of modes when the temperature of the grating is raised by ΔT and when it also experiences a strain ε is given by

$$\frac{\Delta\lambda_i}{\lambda_i} = \left(\frac{1}{\delta n_i}\frac{\partial \delta n_i}{\partial T} + \frac{1}{\Lambda}\frac{\partial \Lambda}{\partial T}\right)\Delta T + \left(\frac{1}{\delta n_i}\frac{\partial \delta n_i}{\partial \varepsilon} + \frac{1}{\Lambda}\frac{\partial \Lambda}{\partial \varepsilon}\right)\varepsilon$$
$$i = 1 \text{ (fundamental)}, 2 \text{ (higher order pair)} \quad (1)$$

The above equations can be solved for temperature and strain provided that the coefficients in the parentheses are known for the specific fibre used. The magnitude of the coefficients in the first pair of parentheses of each equation can be determined by measuring changes in the resonant coupling wavelengths associated with each pair of modes while making controlled changes in the temperature of the fibre. A similar procedure is followed to determine the magnitude of the remaining coefficients by stretching the fibre at constant temperature.

Experiment: The fibre we used for the experiments described in this Letter was an elliptically cored, D-type fibre made by the Andrew Corporation with a measured higher mode cutoff wavelength λ_c equal to 693nm. A polarisation rocking filter with a period of 3mm and extending over 85 coupling points was written using the technique mentioned in [10]. Each coupling point was exposed to 1200 pulses of focused 266nm light from a frequency-quadrupled Nd-YAG laser with a pulse energy of 2.5mJ [11] The spectral coupling efficiency of the rocking filter was examined with a monochromator with a resolution of 0.5nm and a resettability of 0.075nm. Fig. 1*a* shows the polarisation coupling spectrum of the rocking filter unstrained at room temperature. The resonance wavelength λ_1 was 796.2nm while the resonance wavelength λ_2 was 668.9nm. The measured peak polarisation coupling efficiency for the fundamental mode was 23% and the measured FWHM bandwidth was 6.7nm. The measured peak polarisation coupling efficiency of the filter for the first observable higher-order pair of modes was 11% at the peak and the measured FWHM bandwidth was 4.6nm.

The coupler was immersed in an oil bath heated by a large hot plate and the shifts in resonant coupling wavelengths were measured for both pairs of modes at intervals over a range of 155°C above room temperature. The temperature of the oil was monitored with a thermocouple. Fig. 1*c* shows the transmission spectrum of the fibre at the maximum temperature. The shifts in the resonant coupling wavelengths compared to ambient conditions were $\Delta\lambda_1 = -41.4$nm for the fundamental and $\Delta\lambda_2 = -48.2$nm for